(05-023) - Rapid Heat Insulation Assessment of Buildings

Bettemir, Onder Halis [1]

[1] Inonu University

Thermal insulation capacity of building elements such as windows, window frames, exterior walls, roof, and other parts which contact with the outside may deteriorate over time. Care of the users, quality of the workmanship as well as material, and external factors affect the rate of the deterioration. Therefore, the heat insulation performances of the buildings must be monitored frequently. However, manually and physically inspecting the building elements require important amount of workload and it is prone to error. The buildings are frequently imaged by thermal camera in winter in order to measure the heat insulation performances. The heat losses are detected by implementing image analysis techniques. The Otsu threshold algorithm is implemented to determine the threshold value to detect the building elements or spots that cause important amount of heat loss. The building elements which have the most heat loss are detected and they are manually inspected and necessary repairs are executed. The implemented method reduced the workload of the maintenance staff notably and saved important amount of energy by preventing the heat losses.

Keywords: thermal imaging; digital image analysis; sustainability

Evaluación rápida del aislamiento térmico de los edificios

La capacidad de aislamiento térmico de elementos de construcción como ventanas, marcos de ventanas, paredes exteriores, tejado y otras partes que están en contacto con el exterior puede deteriorarse con el tiempo. El cuidado de los usuarios, la calidad de la mano de obra y del material y los factores externos influyen en el ritmo del deterioro. Por lo tanto, las prestaciones de aislamiento térmico de los edificios deben controlarse con frecuencia. Sin embargo, la inspección manual y física de los elementos del edificio requiere una gran cantidad de trabajo y es propensa a errores. Para medir el rendimiento del aislamiento térmico, en invierno se suelen tomar imágenes de los edificios con cámaras térmicas. Las pérdidas de calor se detectan aplicando técnicas de análisis de imágenes. Se aplica el algoritmo de umbral de Otsu para determinar el valor umbral y detectar los elementos o puntos del edificio que causan una pérdida importante de calor. Se detectan los elementos del edificio con mayor pérdida de calor, se inspeccionan manualmente y se realizan las reparaciones necesarias. El método aplicado reduce notablemente la carga de trabajo del personal de mantenimiento y ahorra una cantidad importante de energía al evitar las pérdidas de calor.

Palabras clave: imágenes térmicas; análisis digital de imágenes; sostenibilidad

Correspondencia: Önder Halis Bettemir, onder.bettemir@inonu.edu.tr

1. Introduction

In many countries building inspection companies do not inspect the construction of work items related to thermal insulation of the residential constructions. As a result, reliable data on the thermal insulation quality of the existing building stock is scarce. Moreover, the insulation performance of thermal insulation materials decreases over time. Severe environmental conditions accelerate the worsening of the thermal insulation material. Deterioration of the chemicals that make up the insulation material over time also negatively affects the thermal insulation performance. As a result, a decrease in the thermal insulation performance of a building may occur after 10-15 years after its construction.

Detecting the thermal insulation material directly by visualizing it is a troublesome and damaging process to the building since the thermal insulation material is covered by the plaster. In addition, considering the large number of buildings with unknown thermal insulation performance, performing thermal insulation performance by direct inspection will be both time consuming and very costly. Considering the size of the building stock in large cities, examining the images by human effort and identifying the parts that cause heat loss will not be a feasible method. Instead, it will be faster to identify the sections that cause heat loss with a thermal camera when the building is heated. For this reason, the detection of building sections which cause heat loss should be carried out without human intervention. In the classification process carried out by image processing methods, a threshold value that can be defined as expert opinion is widely used. The threshold value depends very much on the brightness of the environment when the image is taken, the detection level of the camera sensors and the background of the image. For this reason, determination of image specific threshold value by human will slow down measurement efforts (Bettemir, 2020; 2023).

Sensitivity of measurements to detect heat loss with infrared images depends on the emissivity of the surface, the emission of particles in the atmosphere, ambient temperature, wind speed, viewing angle and the distance between the object and the camera (Wardlaw et al., 2010). The indoor and outdoor temperature difference should be at least 10^0C, the wind speed must be at most 5 m/s, and the measured surface must not be exposed to direct solar radiation during image acquisition. Reflections of objects surrounding the windows, inaccurate measurement of sky temperature and the use of low-emissivity glass affect the measurement results (Lucchi, 2018). Ambient temperature, wind speed and distance from the examined object also affect measurement accuracy (Kylili et al., 2014).

Wardlaw et al. (2010) created 3D thermal image of a building with thermal images obtained from different angles and positions with the structure from motion algorithm and manually detected the areas causing heat loss. Hou et al. (2021a) utilized deep convolutional neural network tools and detected heat losses of buildings from optical thermal images obtained by UAV with the Pyramid Scene Parsing Network algorithm. Heat loss areas were determined with DeepLabv3 and ANN with Mask R-CNN architecture using 4190 training and 1000 test images. It has been stated that the most important problem in practice is the identification of vehicles on the street as heat loss points. Hou et al. (2021b) converted optical images into thermal images by simulation using a Generative Adversarial Network-based method. Optical images were converted into thermal equivalents by ANN fed with a training set of 14,000 images. Arjoune et al. (2021) estimated the temperature of the building surface and the cumulative U value of the surface by K-means and threshold-based classification. ANN was trained by 42,439 images obtained by UAV and windows, glass, walls as well as trees were manually determined. Heat transmission coefficients of the elements forming the building facade were estimated with empirical formulas. However, the predicted values were 4 times the actual value for walls and half of the actual value for windows. Pavlović and Barbarić (2013) measured the emissivity of the wall by Thermography Studio software. Heat losses resulting

from moisture, cracks and insufficient thermal insulation were detected manually. In order to improve the accuracy of the results, thermal images are supported with temperature meter data. O'Grady (2018) examined the interaction of multiple thermal bridges formed in windows by thermal imaging. Kim et al. (2021) classified heat losses with the density-based spatial clustering method of noisy applications. ANN was trained by manually detecting 151 thermal bridges and 223 cases from 134 thermal images with 89% and 76% accuracy at best and worst conditions, respectively. Despotovic et al. (2019) estimated the heating energy requirement of the buildings with ANN trained by optical images of the building and architectural elements as well as age of the buildings. To feed the ANN, 2898 images were used for training, 387 images for validation and 580 images for testing. In the analyses, approximately 60% accuracy was achieved.

Martinez et al. (2006) examined the heat losses caused by windows by analysing the images obtained by a thermal camera on the UAV. The emissivity value of the objects was assumed to be 0.8. Heat losses due to window panes were estimated by establishing a statistical model with window frames. Failed solar panel cells are disabled by the operating system and these cells have higher temperatures than others. Regions in photovoltaic cell size and shape that are hotter than their surroundings were determined with an edge detection-based method (Guerriero and Daliento, 2017). Macher et al. (2020) scanned the buildings with a ground vehicle equipped with a combined laser scanner and thermal camera equipment. Plane fitting algorithm is utilized to eliminate objects in front of the building, such as trees and street lamps from the obtained a point cloud. The threshold value to classify as object or background was determined by histogram analysis.

Taylor et al. (2014) utilized HEAT3 heat transfer analysis software to determine the required insulation performances of the buildings and their current thermal insulation performances. Whether there was a workmanship defect was manually determined after the comparison. Gonzalez et al. (2013) utilized Photomodeler Pro v6 software with the affine scale invariant feature transformation algorithm to georeference thermal images. Overlapping thermal images were rendered on the building surface and orthothermal images were created by image processing. Lai et al. (2015) examined the proper operating conditions of the heating and electrical appliances inside the building from the thermal image obtained with a mobile phone. Lewandowski et al. (2018) measured heat losses of buildings by a thermal camera and a vertical heating plate under laboratory conditions. Nikzad et al. (2011) manually determined heat loss, moisture and mold formation in historical buildings from thermal images. Garrido et al. (2018) georeferenced the thermal images using at least 4 control points with photogrammetry. Thermal calculations were made with the 0.95 thermal diffusion coefficients. The image was filtered with a one-dimensional median filter in horizontal and vertical directions. Horizontal and vertical lines were searched and thermal bridge classification was made by considering the thermal transmission value, temperature difference and spatial analysis.

2. Methodology

A framework that determines the threshold value with the Otsu Algorithm and detects the building parts that cause heat loss through binarization without the requirement for any external threshold value is developed. When the buildings are heated from an internal heat source, thermal images of the building is taken from the outside with a thermal camera and image processing techniques are used to detect the building elements that cause heat loss with minimal human intervention. Threshold values were determined by applying the Otsu threshold determination algorithm in two ways. The first way directly applies the Otsu Algorithm to the thermal images, in the second method Otsu threshold determination algorithm is applied to the edge images obtained by applying 12 edge detection operators obtained from the literature.

By applying the threshold value itself, half and a quarter, the success of detecting sections that cause heat loss was examined.

In this study, it is aimed to derive methods to detect heat losses by determining the threshold value without any human intervention. Performances of Integrated Function Algorithm on thermal images with Roberts, Sobel, Prewitt, Robinson, Kirsch, Frei-Chen and modifications on Frei-Chen, Laplace and Kenny edge detection operators compiled from the literature was examined. Masks of the aforementioned methods are presented in Table 1.

Table 1: Implemented edge detection operators

Method	Mask	Magnitude of Edge
Roberts Edge Detection Operator (Cherri and Karim, 1989)	$R_1 = \begin{bmatrix} 1 & 0 \\ 0 & -1 \end{bmatrix}$ $R_2 = \begin{bmatrix} 0 & 1 \\ -1 & 0 \end{bmatrix}$	$M_1 = \sqrt{R_1^2 + R_2^2}$, $M_2 = |R_1| + |R_2|$
Sobel Edge Detection Operator (Kanopoulos et al., 1988)	$S_1 = \begin{bmatrix} -1 & -2 & -1 \\ 0 & 0 & 0 \\ 1 & 2 & 1 \end{bmatrix}$ $S_2 = \begin{bmatrix} -1 & 0 & 1 \\ -2 & 0 & 2 \\ -1 & 0 & 1 \end{bmatrix}$	$M_S = \sqrt{S_1^2 + S_2^2}$
Prewitt Edge Detection Operator (Abdou and Pratt; 1979)	$P_1 = \begin{bmatrix} 1 & 1 & 1 \\ 1 & -2 & 1 \\ -1 & -1 & -1 \end{bmatrix}$ $P_2 = \begin{bmatrix} 1 & 1 & 1 \\ 1 & -2 & -1 \\ 1 & -1 & -1 \end{bmatrix}$ $P_3 = \begin{bmatrix} 1 & 1 & -1 \\ 1 & -2 & -1 \\ 1 & 1 & -1 \end{bmatrix}$ $P_4 = \begin{bmatrix} 1 & -1 & -1 \\ 1 & -2 & -1 \\ 1 & 1 & 1 \end{bmatrix}$ $P_5 = \begin{bmatrix} -1 & -1 & -1 \\ 1 & -2 & 1 \\ 1 & 1 & 1 \end{bmatrix}$ $P_6 = \begin{bmatrix} -1 & -1 & 1 \\ -1 & -2 & 1 \\ 1 & 1 & 1 \end{bmatrix}$ $P_7 = \begin{bmatrix} -1 & 1 & 1 \\ -1 & -2 & 1 \\ -1 & 1 & 1 \end{bmatrix}$ $P_8 = \begin{bmatrix} 1 & 1 & 1 \\ -1 & -2 & 1 \\ -1 & -1 & 1 \end{bmatrix}$	$M_P = MAX\left(\sum_{i=1}^{8} P_i\right)$
Robinson Edge Detection Operator (Robinson, 1977)	$R_W = \begin{bmatrix} 1 & 2 & 1 \\ 0 & 0 & 0 \\ -1 & -2 & -1 \end{bmatrix}$ $R_{NW} = \begin{bmatrix} 0 & 1 & 2 \\ -1 & 0 & 1 \\ -2 & -1 & 0 \end{bmatrix}$ $R_N = \begin{bmatrix} -1 & 0 & 1 \\ -2 & 0 & 2 \\ -1 & 0 & 1 \end{bmatrix}$ $R_{NE} = \begin{bmatrix} -2 & -1 & 0 \\ -1 & 0 & 1 \\ 0 & 1 & 2 \end{bmatrix}$ $R_E = \begin{bmatrix} -1 & -2 & -1 \\ 0 & 0 & 0 \\ 1 & 2 & 1 \end{bmatrix}$ $R_{SE} = \begin{bmatrix} 0 & -1 & -2 \\ 1 & 0 & -1 \\ 2 & 1 & 0 \end{bmatrix}$ $R_S = \begin{bmatrix} 1 & 0 & -1 \\ 2 & 0 & -2 \\ 1 & 0 & -1 \end{bmatrix}$ $R_{SW} = \begin{bmatrix} 2 & 1 & 0 \\ 1 & 0 & -1 \\ 0 & -1 & -2 \end{bmatrix}$	$M_R = MAX\left(\sum_{i=1}^{8} R_i\right)$
Kirsch Edge Detection Operator (Patel et al., 2016)	$K_1 = \begin{bmatrix} -3 & -3 & 5 \\ -3 & 0 & 5 \\ -3 & -3 & 5 \end{bmatrix}$ $K_2 = \begin{bmatrix} -3 & 5 & 5 \\ -3 & 0 & 5 \\ -3 & -3 & -3 \end{bmatrix}$ $K_3 = \begin{bmatrix} 5 & 5 & 5 \\ -3 & 0 & -3 \\ -3 & -3 & -3 \end{bmatrix}$ $K_4 = \begin{bmatrix} 5 & 5 & -3 \\ 5 & 0 & -3 \\ -3 & -3 & -3 \end{bmatrix}$ $K_5 = \begin{bmatrix} 5 & -3 & -3 \\ 5 & 0 & -3 \\ 5 & -3 & -3 \end{bmatrix}$ $K_6 = \begin{bmatrix} -3 & -3 & -3 \\ 5 & 0 & -3 \\ 5 & 5 & -3 \end{bmatrix}$ $K_7 = \begin{bmatrix} -3 & -3 & -3 \\ -3 & 0 & -3 \\ 5 & 5 & 5 \end{bmatrix}$ $K_8 = \begin{bmatrix} -3 & -3 & -3 \\ -3 & 0 & 5 \\ -3 & 5 & 5 \end{bmatrix}$	$M_K = MAX\left(\sum_{i=1}^{8} K_i\right)$
Frei-Chen Edge Detection Operator (Frei and Chen, 1977)	$W_1 = \begin{bmatrix} 1 & \sqrt{2} & 1 \\ 0 & 0 & 0 \\ -1 & -\sqrt{2} & -1 \end{bmatrix}$ $W_2 = \begin{bmatrix} 1 & 0 & -1 \\ \sqrt{2} & 0 & -\sqrt{2} \\ 1 & 0 & -1 \end{bmatrix}$ $W_3 = \begin{bmatrix} 0 & -1 & \sqrt{2} \\ 1 & 0 & -1 \\ -\sqrt{2} & 1 & 0 \end{bmatrix}$ $W_4 = \begin{bmatrix} \sqrt{2} & -1 & 0 \\ -1 & 0 & 1 \\ 0 & 1 & -\sqrt{2} \end{bmatrix}$ $W_5 = \begin{bmatrix} 0 & 1 & 0 \\ -1 & 0 & 1 \\ 0 & 1 & 0 \end{bmatrix}$ $W_6 = \begin{bmatrix} -1 & 0 & 1 \\ 0 & 0 & 0 \\ 1 & 0 & -1 \end{bmatrix}$ $W_7 = \begin{bmatrix} 1 & -2 & 1 \\ -2 & 4 & -2 \\ 1 & -2 & 1 \end{bmatrix}$ $W_8 = \begin{bmatrix} -2 & 1 & -2 \\ 1 & 4 & 1 \\ -2 & 1 & -2 \end{bmatrix}$ $W_9 = \begin{bmatrix} 1 & 1 & 1 \\ 1 & 1 & 1 \\ 1 & 1 & 1 \end{bmatrix}$	$e = \left(\dfrac{\sum_{i=1}^{4} R_i}{\sum_{i=1}^{9} R_i}\right)$
Modified Frei-Chen Edge Detection Operator (Feng et al., 2017)	$A_x = \begin{bmatrix} 1 & 0 & -1 \\ \sqrt{2} & 0 & -\sqrt{2} \\ 1 & 0 & -1 \end{bmatrix}$ $A_Y = \begin{bmatrix} 1 & \sqrt{2} & 1 \\ 0 & 0 & 0 \\ -1 & -\sqrt{2} & -1 \end{bmatrix}$ $A_{45} = \begin{bmatrix} \sqrt{2} & -1 & 0 \\ -1 & 0 & 1 \\ 0 & 1 & -\sqrt{2} \end{bmatrix}$ $A_{135} = \begin{bmatrix} 0 & 1 & -\sqrt{2} \\ -1 & 0 & 1 \\ \sqrt{2} & -1 & 0 \end{bmatrix}$	$A = \sqrt{\dfrac{1}{2\sqrt{2}}\left[A_X^2 + A_Y^2 + A_{45}^2 + A_{135}^2\right]}$
Modified Frei-Chen Edge Detection Operator II (Park, 1999)	$R_V = \begin{bmatrix} -1 & -1 & -1 \\ 3 & 0 & 3 \\ -1 & -1 & -1 \end{bmatrix}$ $R_{LD} = \begin{bmatrix} -1 & -1 & 3 \\ -1 & 0 & -1 \\ 3 & -1 & -1 \end{bmatrix}$ $R_H = \begin{bmatrix} -1 & 3 & -1 \\ -1 & 0 & -1 \\ -1 & 3 & -1 \end{bmatrix}$ $R_{RD} = \begin{bmatrix} 3 & -1 & -1 \\ -1 & 0 & -1 \\ -1 & -1 & 3 \end{bmatrix}$	$R = \sqrt{\dfrac{1}{12}\left[R_V^2 + R_{LD}^2 + R_H^2 + R_{RD}^2\right]}$

Laplace Edge Detection Algorithm (Vliet et al., 1988)	$L_X = \begin{bmatrix} 0 & -1 & 0 \\ -1 & 4 & -1 \\ 0 & -1 & 0 \end{bmatrix}$ $L_Y = \begin{bmatrix} -1 & -1 & -1 \\ -1 & 8 & -1 \\ -1 & -1 & -1 \end{bmatrix}$	$L = MAX\left(\left|L_X\right|,\left|L_Y\right|\right)$
2nd Degree Laplace Edge Detection Algorithm (Qu and Zhang, 2010)	$G = \frac{1}{8}\begin{bmatrix} 0 & 1 & 0 & 1 & 0 \\ 1 & 4 & 8 & 4 & 1 \\ 0 & 8 & -56 & 8 & 0 \\ 1 & 4 & 8 & 4 & 1 \\ 0 & 1 & 0 & 1 & 0 \end{bmatrix}$	
Integrated Function Algorithm (White and Rohrer; Trier and Taxt, 1995)	$A(i,j) = \sum_{n=-1,0,1}\sum_{m=-1,,0,1} a(i+n, j+m)$ $a(i,j), \left|u(i-1,j)-u(i+1,j)\right|+\left|u(i,j-1)-u(i,j+1)\right|$ $ddxy(i,j) = u(i+2,j)+u(i-2,j)+u(i,j+2)+u(i,j-2)-4u(i,j)$	$S(i,j) = \begin{cases} 0 & if \quad A(i,j)<T \\ - & if \quad A(i,j)\ge T \ and \ ddxt(i,j)<0 \\ + & if \quad A(i,j)\ge T \ and \ ddxt(i,j)\ge 0 \end{cases}$ heat loss is searched among the "+-" and "-+" patterns
Canny Edge Detection Algorithm (Ding and Goshtasby, 2001; Rong et al., 2014). Filtered by	$G = \begin{bmatrix} 2 & 4 & 5 & 4 & 2 \\ 4 & 9 & 12 & 9 & 4 \\ 5 & 12 & 15 & 12 & 5 \\ 4 & 9 & 12 & 9 & 4 \\ 2 & 4 & 5 & 4 & 2 \end{bmatrix}$	Sobel operator is implemented to detect continuous edges.

Magnitudes of the edges computed by the methods presented in Table 1 are compared by the threshold value obtained by Otsu threshold algorithm and the successes of the methods for the detection of heat loss regions are compared. Otsu algorithm aims to determine a threshold value to classify the image into two classes: background and the examined object. The method searches for the threshold that maximizes the average of the image values that make up the background and the object. If there are L gray levels in the image and the number of image elements at the ith brightness level is n_1, n_2, …, n_L, then i = [1,2,3,..,L] and $n_1 + n_2 + … + n_L = N$ where N is the number of image elements that make up the image.

Probability of an image element being at the ith brightness level is expressed as $P_i = \frac{n_i}{N}$. If the threshold value is equal to k, image elements with the value [1, 2, …, k] are included in the S_0 class and image elements [k+1, …, L-1, L] are included in the S_1 class. Probability of an image element belonging to S_0 and S_1 classes is presented in Eq. 1 (Otsu, 1979).

$$w_0 = \Pr\left(S_0\right) = \sum_{i=1}^{k} P_i = w(k), \quad w_1 = \Pr\left(S_1\right) = \sum_{i=k+1}^{L} P_i = 1 - w(k) \tag{1}$$

In Eq. 1 w_0 term expresses the probability of any pixel of the image having a brightness value between 1 and k. The mentioned event is the probability of the considered pixel to belong to the S_0 class. The average of the brightness values of the pixels included in the class is computed as given in Eq. 2.

$$\mu_0 = \sum_{i=1}^{k}\left(i * \Pr(i \mid S_0)\right) = \sum_{i=1}^{k}\left(i * \frac{P_i}{w_0}\right) = \frac{\mu(k)}{w(k)} \tag{2}$$

In Eq. 2 $\mu(k)$ is computed by the $\sum_{i=1}^{k} i * P_i$ expression whereas $w(k)$ is computed by $\sum_{i=1}^{k} P_i$.

Average of the S_1 class is computed by $\mu_1 = \sum_{i=1+k}^{L}(i * \Pr(i \mid S_1)) = \sum_{i=k+1}^{L}\left(i * \frac{P_i}{w_1}\right) = \frac{\mu_T - \mu(k)}{1 - w(k)}$. where

$\mu_T = \mu(L) = \sum_{i=1}^{L} i * P_i$. Variance of S_0 class is computed by the expression given in Eq. 3.

$$\sigma_0^2 = \sum_{i=1}^{k}(1 - \mu_0)^2 \Pr(i \mid S_0) = \sum_{i=1}^{k}(1 - \mu_0)^2 \frac{P_i}{w_0} \qquad (3)$$

Variance of S_1 class is computed by $\sigma_1^2 = \sum_{i=k+1}^{L}(1 - \mu_1)^2 \frac{P_i}{w_1}$. Difference of the variances of the two

class is aimed to be maximized which can be achieved by the expression given in Eq. 4.

$$\sigma_B^2(k) = \frac{[\mu_T w(k) - \mu(k)]^2}{w(k)[1 - w(k)]} \qquad (4)$$

Otsu threshold algorithm is implemented on the edge images obtained by the methods illustrated in Table 1 to compare the success of the detection of thermal heat loss.

3. Case Study
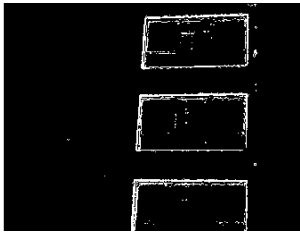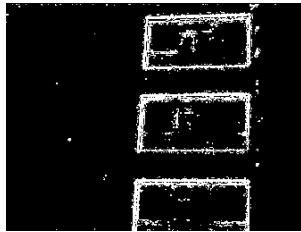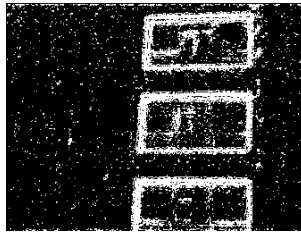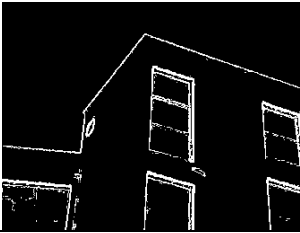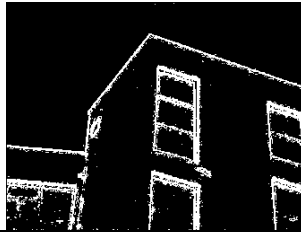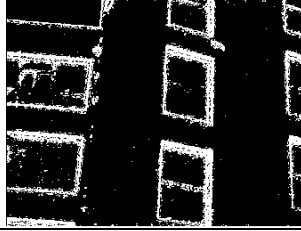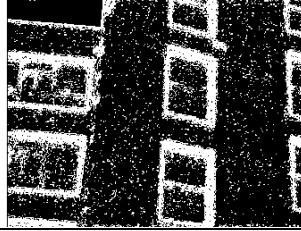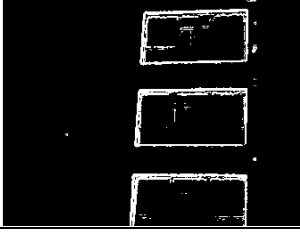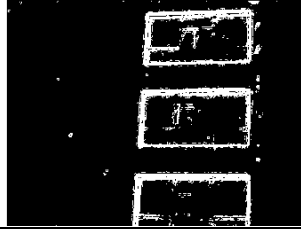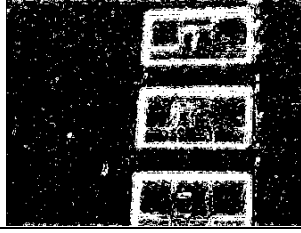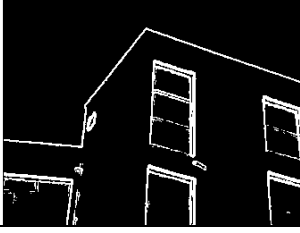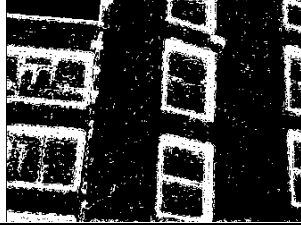
Thermal images shown in Figure 1 are acquired by FLIR thermal camera on 27th January 2022 at around 19:50 when the air temperature was 4^0C. Building facades of the buildings of faculty of engineering of İnönü University were imaged. The buildings were subjected to indoor heating during the imaging and the indoor temperatures were varying between 22 and 23^0C. Exterior surface of the imaged buildings were insulated by XPS sidings. Resolution of the thermal images is 256x336 and has 8 bits of spectral resolution.
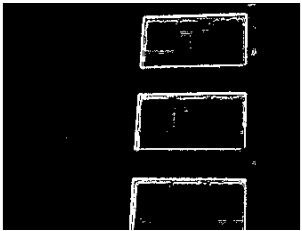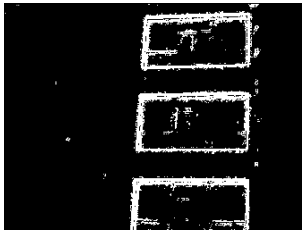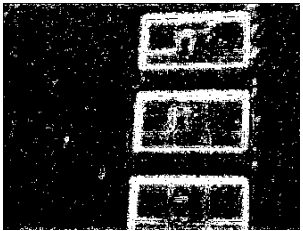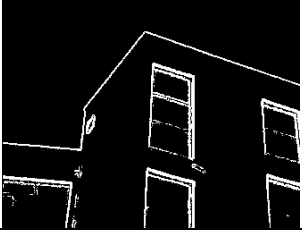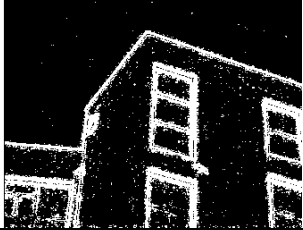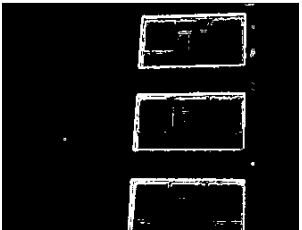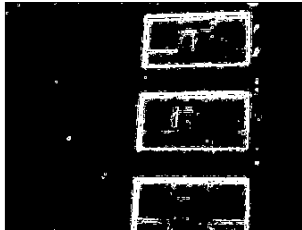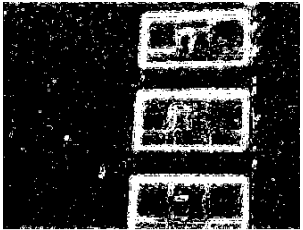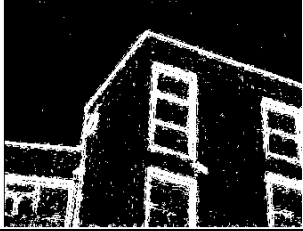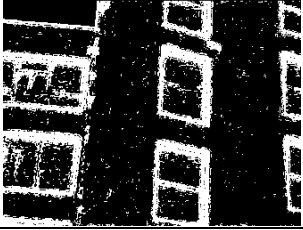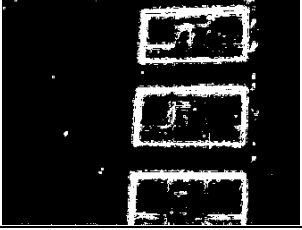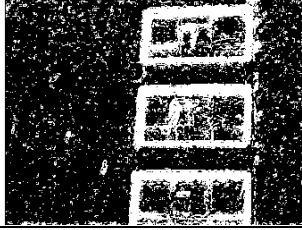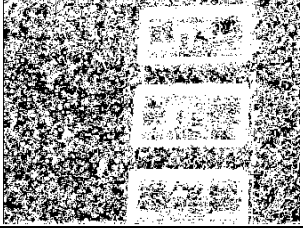
Figure 1: Acquired thermal images

(a)   (b)   (c)
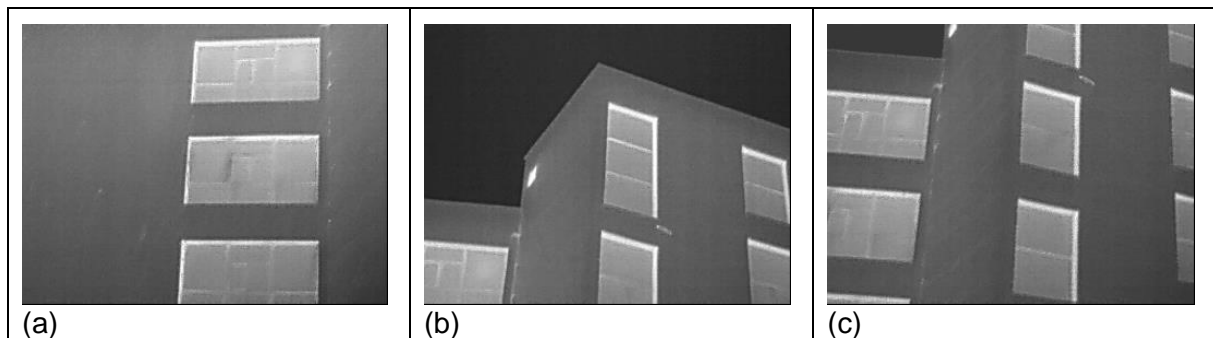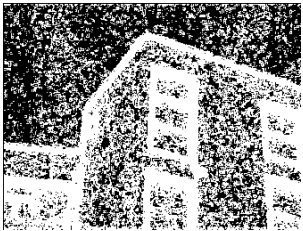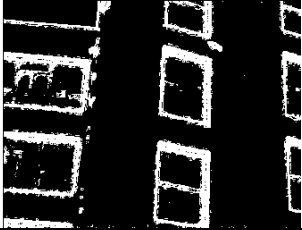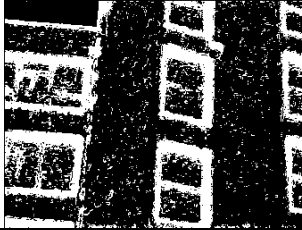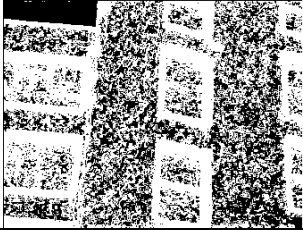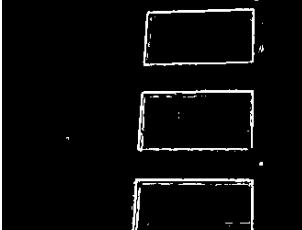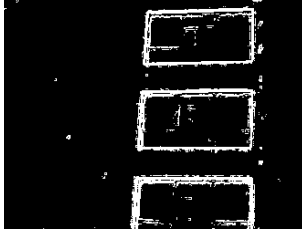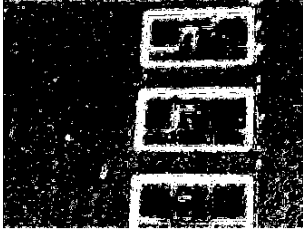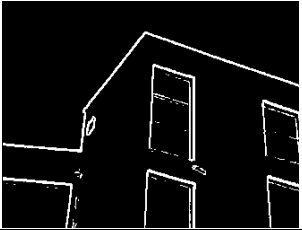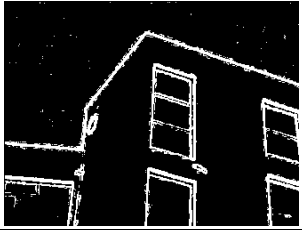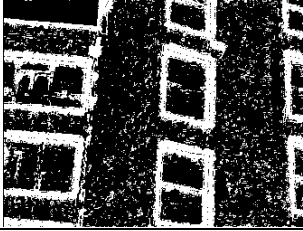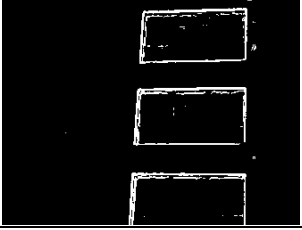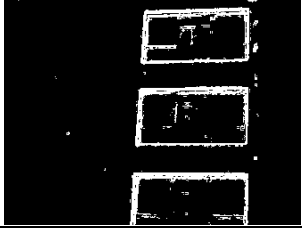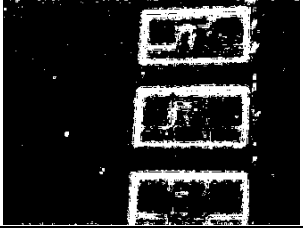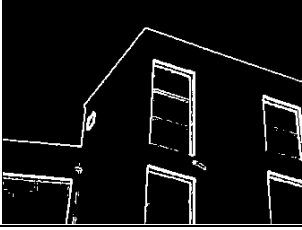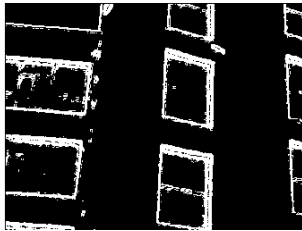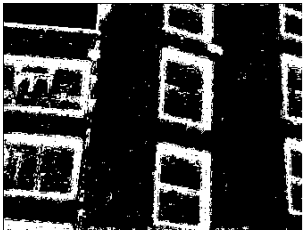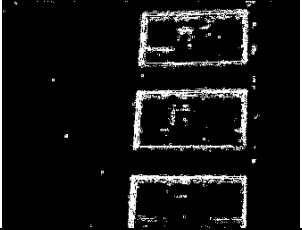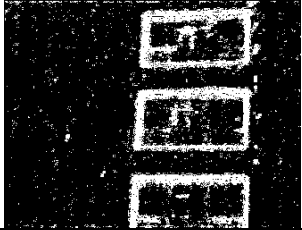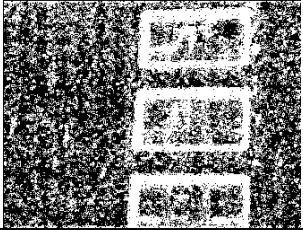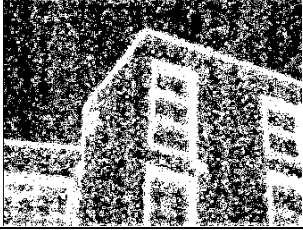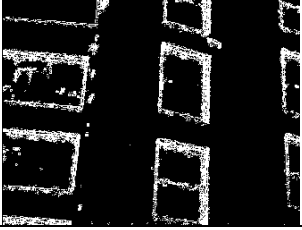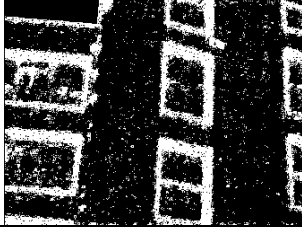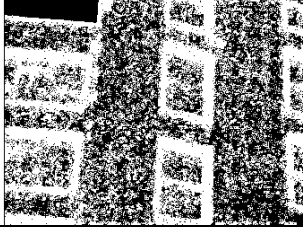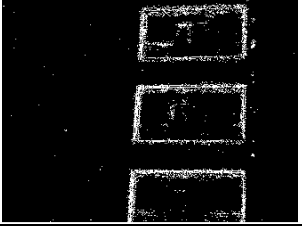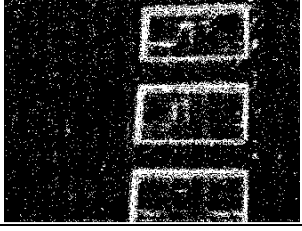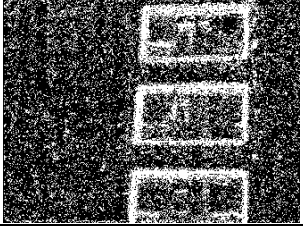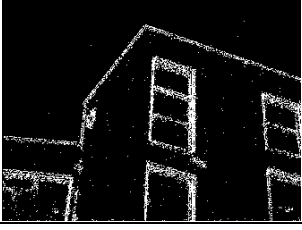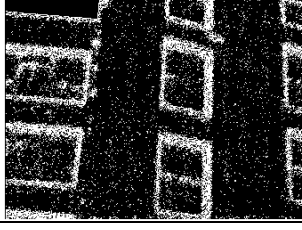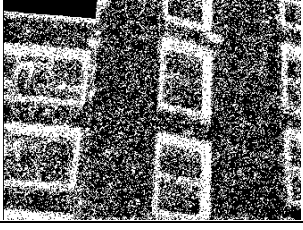
Edge detection algorithms presented in Table 1 are implemented on the thermal images and edge images are obtained. Otsu threshold algorithm is executed to define threshold values for each edge image. The edge image is binarized by the corresponding threshold value. Computations are executed on MatLAB software. Obtained binarized images are presented in Figure 2 where the white pixels are the regions of the building in which heat loss occurs.
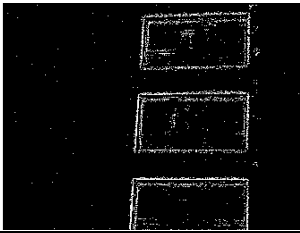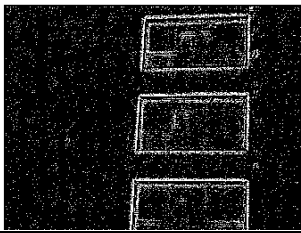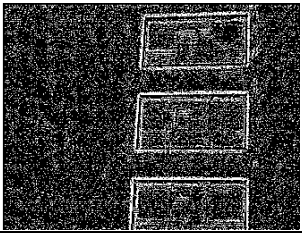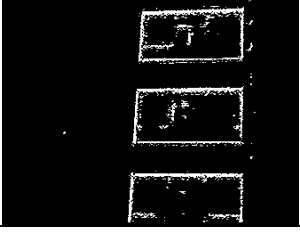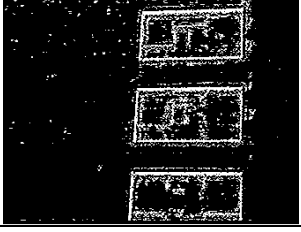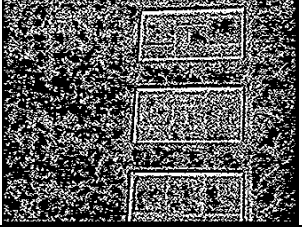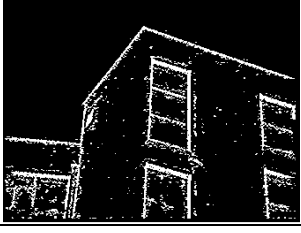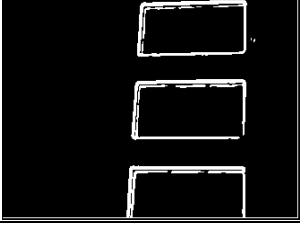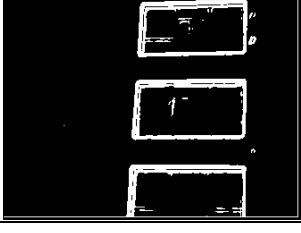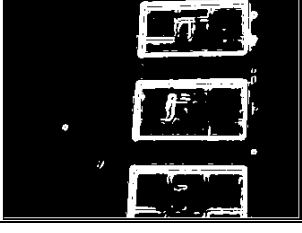
Figure 2: Resulting edge images

Method	Otsu	Otsu 0.5	Otsu 0.25
Roberts Image 1			
Roberts Image 2			
Roberts Image 3			
Sobel Image 1			
Sobel Image 2			
Sobel Image 3			

Prewitt Image 1			
Prewitt Image 2			
Prewitt Image 3			
Robinson Image 1			
Robinson Image 2			
Robinson Image 3			
Kirsch Image 1			

Kirsch Image 2			
Kirsch Image 3			
Frei-Chen Image 1			
Frei-Chen Image 2			
Frei-Chen Image 3			
Modified Frei-Chen Image 1			
Modified Frei-Chen Image 2			

Modified Frei-Chen Image 3			
Modified Frei-Chen II Image 1			
Modified Frei-Chen II Image 2			
Modified Frei-Chen II Image 3			
Laplace Image 1			
Laplace Image 2			
Laplace Image 3			

2nd Degree Laplace Image 1			
2nd Degree Laplace Image 2			
2nd Degree Laplace Image 3			
IFA Image 1			
IFA Image 2			
IFA Image 3			
Canny Image 1			

Canny Image 2			
Canny Image 3			

Otsu threshold algorithm detected threshold values successfully for all of the edge images. Further reduction of the Otsu threshold enlarges number of pixels classifies as the heat loss building portion as expected. However, some of the edge algorithms provide noisy results and some of them provide cleaner classification results depending on the magnitude resulting edge images.

Roberts operator provides sharp edge images for the 1 Otsu threshold value and noisy images especially for 0.25 Otsu threshold values. Especially, for the second image some of the air section is classified as heat loss portion. Sobel operator provides sharper edge images than Roberts operator due to its larger mask which filters some of the noises in the images. Prewitt operator can be classified as in between the Roberts and Sobel operators. Prewitt operator cannot detect the aluminium window frames successfully. Robinson operator is better than Sobel operator as the Robinson operator considers all of the directions in 45^0.

Magnitude of the Kirsch operator is very high; therefore its edge image covers significantly large area as heat loss region for 1 Otsu threshold value. Window frames are successfully detected in 1 Otsu threshold value and noise becomes dominant for lower threshold value. Original Frei-Chen operator provides successful results with sharp edge images. Original Frei-Chen can also be used by 0.5 Otsu threshold value but noise of the image becomes apparent. First Modification on the Frei-Chen algorithm is better than the Original Frei-Chen so that when utilized by 1 and 0.5 Otsu threshold value sharp images with very little noise can be obtained. The metric successfully detects the window frames and the wall insulation with workmanship errors such as where the scaffolding is ties on the exterior wall. Second Modification on the Frei-Chen Algorithm increases the Edge Magnitude significantly and this operator contain important amount of noise even in 1 Otsu threshold value.

Laplace operator cannot provide continuous edge lines and therefore it is difficult to detect lines from the edge images. Assigning lower threshold values such as 0.5 and 0.25 Otsu threshold values increases the noise in the images. Especially in the second image significant number of pixels representing air is classified as heat loss portion for lower Otsu threshold value. Second degree Laplace operator provides slightly better edge images than Laplace operator but the magnitude of the noise is still high. Therefore, lower threshold values provide erroneous classifications due to noise.

IFA provides less noisy edge images than Laplace algorithms. The qualities of the classified images are not deteriorated for 0.5 Otsu threshold value. On the other hand, discontinued edges exist especially at the window frames. Canny operator provides the least noisy images due to its filtering mask. Therefore, this operator presents smooth images for lower threshold values. The filtering also removes some of the real heat loss regions for this reason this operator is better to be implemented with lower Otsu threshold. However, some of the

workmanship errors are removed because of the filtering task, while nowhere in the air is classified as heat loss region.

4. Discussion of Results

Examination on the Otsu threshold values show that the 0.25 Otsu threshold classifies many portions as heat loss. Some of the methods with high edge magnitudes classify even the air as heat loss portion which may be caused by the uprising relatively hot air due to the heat loss from the building facade and roof. Consequently, 0.25 Otsu threshold may lead to false heat loss detections due to its oversensitivity. 0.5 Otsu threshold value does not provide as scattered images as 0.25 Otsu threshold but successfully detects defects on the walls caused by the poor workmanship or ignorance during the construction. Some of the connection spots on the wall to stabilize the scaffolding are detected. Heat insulation material cannot be covered on these regions because of the connection rods penetrated into the wall and after the dismantling of the scaffolding the spot is plastered and painted which leads to poor heat insulation. Mentioned spots are detected more successfully when the Otsu threshold value is applied. However, 0.5 Otsu threshold still classifies air as heat loss building portion if high magnitude edge detection methods are implemented. Original Otsu threshold value provides the most smooth and clear binary images. Moreover, original Otsu detects most of the defects on the walls.

Kirsch, Laplace, 2nd degree of Laplace, and Modified Frei Chen II edge detection operators provided the worst results among the examined edge detection algorithms. The aforementioned edge detection operators provided fuzzy and scattered heat loss regions. This is because the algorithms provide very high edge magnitudes and small differences in thermal emissivity is enlarged and classified as heat loss. Consequently, significantly many scattered pixels are classified as heat loss region around the window frames. On the other hand, the aforementioned methods are the only ones to distinguish the difference of heat loss between the glass and the window frames. Roberts, Sobel, Modified Frei-Chen, and Integrated Function Algorithm methods presented moderate success. Their output images were semi blurred therefore building and window borders were not sharp. Prewitt, Robinson, Frei-Chen, and Canny methods presented the best results among the tested methods. The resulting classification detected the defects on the walls as well as building and window borders were sharp enough to be detected by a line detection algorithm. However, due to filtering Canny cannot detect all of the defects on the wall.

5. Conclusion

In this study, improperly insulated portions of the buildings are aimed to be detected by analyzing the thermal images without human intervention. In order to classify the improperly insulated portions, edge detection algorithms are implemented and Otsu threshold determination algorithm detects the most suitable threshold value for the classification of heat loss portions. Previous study on the subject revealed that the edge images provide more stable and sharp images compared with original images. In this study, Otsu threshold algorithm is implemented on edge images obtained by 12 edge detection algorithms derived from the literature. Each edge detection algorithm is tested on 3 test images acquired at İnönü University. Different coefficients of Otsu threshold value are applied to measure the effect of the threshold value. The analysis revealed that Otsu threshold provides stable results for all of the edge detection algorithms with small deviations. Moreover, edge detection algorithms with high edge magnitude present false edges and may classify air as heat loss region. Even though the aforementioned shortcomings, Otsu Threshold algorithm provided satisfactory results for the detection of heat loss building portions without human intervention. The autonomous

extraction of window frames as well as defects on the walls and area computation of the poorly insulated area can be executed as future study.

References

Abdou, I. E., & Pratt, W. K. (1979). Quantitative design and evaluation of enhancement/thresholding edge detectors. Proceedings of the IEEE, 67(5), 753-763.

Arjoune, Y., Peri, S., Sugunaraj, N., Biswas, A., Sadhukhan, D., & Ranganathan, P. (2021). An instance segmentation and clustering model for energy audit assessments in built environments: A multi-stage approach. Sensors, 21(13), 4375.

Bettemir, Ö.H. (2020). Bazı Yerel Benirizasyon Yöntemleri İle Binaların Isı Kaybına Yol Açan Kısımların Belirlenmesi. Computer Science, 5(1), 22-30.

Bettemir, Ö.H. (2023). Kızıl Ötesi Görüntülerden Binalardaki Isı Köprüsünün Belirlenmesi. Politeknik Dergisi, 1-1.

Chen, C. C. (1977). Fast boundary detection: A generalization and a new algorithm. IEEE Transactions on computers, 100(10), 988-998.

Cherri, A. K., & Karim, M. A. (1989). Optical symbolic substitution: edge detection using Prewitt, Sobel, and Roberts operators. Applied optics, 28(21), 4644-4648.

Despotovic, M., Koch, D., Leiber, S., Doeller, M., Sakeena, M., & Zeppelzauer, M. (2019). Prediction and analysis of heating energy demand for detached houses by computer vision. Energy and Buildings, 193, 29-35.

Ding, L., & Goshtasby, A. (2001). On the Canny edge detector. Pattern recognition, 34(3), 721-725.

Feng, Y., Zhang, J., & Wang, S. (2017, October). A new edge detection algorithm based on Canny idea. In AIP Conference Proceedings (Vol. 1890, No. 1). AIP Publishing.

Garrido, I., Lagüela, S., Arias, P., & Balado, J. (2018). Thermal-based analysis for the automatic detection and characterization of thermal bridges in buildings. Energy and Buildings, 158, 1358-1367.

González-Aguilera, D., Lagueela, S., Rodríguez-Gonzálvez, P., & Hernández-López, D. (2013). Image-based thermographic modeling for assessing energy efficiency of buildings façades. Energy and Buildings, 65, 29-36.

Guerriero, P., & Daliento, S. (2017, June). Automatic edge identification for accurate analysis of thermographic images of solar panels. In 2017 6th International Conference on Clean Electrical Power (ICCEP) (pp. 768-772). IEEE.

Hou, Y., Chen, M., Volk, R., & Soibelman, L. (2021a). An approach to semantically segmenting building components and outdoor scenes based on multichannel aerial imagery datasets. Remote Sensing, 13(21), 4357.

Hou, Y., Volk, R., & Soibelman, L. (2021b). A novel building temperature simulation approach driven by expanding semantic segmentation training datasets with synthetic aerial thermal images. Energies, 14(2), 353.

Kanopoulos, N., Vasanthavada, N., & Baker, R. L. (1988). Design of an image edge detection filter using the Sobel operator. IEEE Journal of solid-state circuits, 23(2), 358-367.

Kim, C., Choi, J. S., Jang, H., & Kim, E. J. (2021). Automatic detection of linear thermal bridges from infrared thermal images using neural network. Applied Sciences, 11(3), 931.

Kylili, A., Fokaides, P. A., Christou, P., & Kalogirou, S. A. (2014). Infrared thermography (IRT) applications for building diagnostics: A review. Applied Energy, 134, 531-549.

Lai, J. H. L., Lin, C. C., Chen, C. F. R., & Lin, C. Y. (2015, December). Multi-modality Mobile Image Recognition Based on Thermal and Visual Cameras. In 2015 IEEE International Symposium on Multimedia (ISM) (pp. 477-482). IEEE.

Lewandowski, W. M., Ryms, M., & Denda, H. (2018). Quantitative study of free convective heat losses from thermodynamic partitions using Thermal Imaging. Energy and Buildings, 167, 370-383.

Lucchi, E. (2018). Applications of the infrared thermography in the energy audit of buildings: A review. Renewable and Sustainable Energy Reviews, 82, 3077-3090.

Macher, H., Landes, T., & Grussenmeyer, P. (2020, August). Automation of thermal point clouds analysis for the extraction of windows and thermal bridges of building facades. In XXIV ISPRS Congress (2020 edition) (Vol. 43).

Martinez-De Dios, J. R., & Ollero, A. (2006, July). Automatic detection of windows thermal heat losses in buildings using UAVs. In 2006 world automation congress (pp. 1-6). IEEE.

Nikzad, S., Kari, B. M., & Tahmasebi, F. (2011, April). The application of thermal imaging as a nondestructive test in historic buildings. FEUP.

O'Grady, M., Lechowska, A. A., & Harte, A. M. (2018). Application of infrared thermography technique to the thermal assessment of multiple thermal bridges and windows. Energy and Buildings, 168, 347-362.

Otsu, N. (1975). A threshold selection method from gray-level histograms. Automatica, 11(285-296), 23-27.

Park, R. H. (1999). One-dimensional frequency domain interpretation of compass roof edge and Frei–Chen line masks. Pattern recognition letters, 20(3), 281-284.

Patel, B., Maheshwari, R. P., & Raman, B. (2016). Compass local binary patterns for gender recognition of facial photographs and sketches. Neurocomputing, 218, 203-215.

Pavlović, A., & Barbarić, Ž. (2013). Application of G100/120 thermal imaging camera in energy efficiency measuring in building construction. Serbian Journal of Electrical Engineering, 10(1), 153-164.

Qu, Z., & Zhang, L. (2010, August). Research on image segmentation based on the improved Otsu algorithm. In 2010 Second International Conference on Intelligent Human-Machine Systems and Cybernetics (Vol. 2, pp. 228-231). IEEE.

Rakha, T., & Gorodetsky, A. (2018). Review of Unmanned Aerial System (UAS) applications in the built environment: Towards automated building inspection procedures using drones. Automation in construction, 93, 252-264.

Robinson, G. S. (1977). Edge detection by compass gradient masks. Computer graphics and image processing, 6(5), 492-501.

Rong, W., Li, Z., Zhang, W., & Sun, L. (2014, August). An improved CANNY edge detection algorithm. In 2014 IEEE international conference on mechatronics and automation (pp. 577-582). IEEE.

Taylor, T., Counsell, J., & Gill, S. (2014). Combining thermography and computer simulation to identify and assess insulation defects in the construction of building façades. Energy and Buildings, 76, 130-142.

Trier, Ø. D., & Taxt, T. (1995). Improvement of "integrated function algorithm" for binarization of document images. Pattern Recognition Letters, 16(3), 277-283.

Van Vliet, L. J., Young, I. T., & Beckers, G. L. (1988). An edge detection model based on non-linear laplace filtering. In Machine Intelligence and Pattern Recognition (Vol. 7, pp. 63-73). North-Holland.

Wardlaw, J., Gryka, M., Wanner, F., Brostow, G., & Kautz, J. (2010). A new approach to thermal imaging visualisation. EngD Group Project, University College London.

White, J. M., & Rohrer, G. D. (1983). Image thresholding for optical character recognition and other applications requiring character image extraction. IBM Journal of research and development, 27(4), 400-411.